Biomimetic engineered muscle with capacity for vascular integration and functional maturation in vivo

Mark Juhas[a], George C. Engelmayr, Jr.[a], Andrew N. Fontanella[a], Gregory M. Palmer[b], and Nenad Bursac[a,1]

[a]Department of Biomedical Engineering, Duke University, Durham, NC 27708; and [b]Department of Radiation Oncology, Duke University School of Medicine, Durham, NC 27710

Tissue-engineered skeletal muscle can serve as a physiological model of natural muscle and a potential therapeutic vehicle for rapid repair of severe muscle loss and injury. Here, we describe a platform for engineering and testing highly functional biomimetic muscle tissues with a resident satellite cell niche and capacity for robust myogenesis and self-regeneration in vitro. Using a mouse dorsal window implantation model and transduction with fluorescent intracellular calcium indicator, GCaMP3, we nondestructively monitored, in real time, vascular integration and the functional state of engineered muscle in vivo. During a 2-wk period, implanted engineered muscle exhibited a steady ingrowth of blood-perfused microvasculature along with an increase in amplitude of calcium transients and force of contraction. We also demonstrated superior structural organization, vascularization, and contractile function of fully differentiated vs. undifferentiated engineered muscle implants. The described in vitro and in vivo models of biomimetic engineered muscle represent enabling technology for novel studies of skeletal muscle function and regeneration.

tissue engineering | contractile force | self-repair | angiogenesis | window chamber

Natural skeletal muscle consists of terminally differentiated, highly aligned, and contractile myofibers and a population of resident muscle stem cells, known as satellite cells (SCs), that are indispensable for muscle growth (1) and regeneration (2). The ability to create engineered muscle tissues that mimic the structural, functional, and regenerative properties of native muscle would enable design of accurate in vitro models for studies of muscle physiology and development (3, 4) and promote cell-based therapies for muscle injury and disease (5, 6). Pioneering studies of Vandenburgh and coworkers (7) and Dennis and Kosnik (8) were the first to demonstrate in vitro engineering of functional mammalian muscle constructs, followed by other studies reporting that differentiated engineered muscle can survive and vascularize upon implantation in vivo (9–13). Simultaneously, various studies have shown that, compared with differentiated or committed cells, undifferentiated SCs are a more potent myogenic cell source, with the ability to engraft and replenish the host satellite cell pool and support future rounds of muscle regeneration (14–16). Thus, it is likely that, for optimal therapy, engineered muscle tissues should fully recreate the cellular heterogeneity of native muscle and consist of both force-generating, differentiated myofibers and a functioning SC pool to allow further maturation and regeneration in vivo. Additionally, for long-term survival and efficient repair, implanted engineered muscle constructs must rapidly integrate into host vascular system and significantly increase their functional output compared with preimplantation levels.

In this study, we used primary rat myogenic cells to engineer skeletal muscle tissues with highly organized architecture and force-generating capacity comparable with those of native muscle. We characterized the temporal dynamics of myogenic processes within engineered muscle and documented the in vitro formation of a homeostatic tissue state with the coexistence of highly contractile muscle fibers and functional satellite cells. To continuously

monitor engineered tissue survival, function, and vascularization after implantation, we transduced myogenic cells with GCaMP3, a genetic indicator of intracellular Ca^{2+} concentration used previously in neurobiological (17) and cardiac (18) research, and implanted the muscle constructs in a dorsal skinfold chamber in nude mice. The use of this minimally invasive, in vivo platform allowed us to simultaneously, in real time, quantify and compare changes in Ca^{2+} transient amplitude and vascular density between highly differentiated and undifferentiated engineered muscle implants and to further assess the maintenance of satellite cell pool and enhancement of contractile function relative to those preimplantation. Overall, our studies describe important advances in the field of skeletal muscle tissue engineering and lay the foundation for novel studies of cellular function and signaling in a physiological environment in real time.

Results

Structure of Engineered Muscle. Engineered muscle bundles (Fig. 1A) were created using a neonatal rat myogenic cell population that predominantly consisted of activated SCs, positive for paired box 7 (Pax7) and myogenic differentiation (MyoD) proteins, and a small fraction of myogenin+ precursors, but no evidence of endothelial or smooth-muscle cells (SI Appendix, Fig. S1). After 2 wk of culture, engineered bundles consisted of laminin-surrounded myofibers that occupied the entire tissue volume (Fig. 1B) and a peripheral layer of vimentin+ fibroblasts that resembled the epimysial connective tissue layer encasing the myofibers of neonatal hindlimb muscle (SI Appendix, Fig. S2A). The interior of both engineered and native neonatal muscle contained densely packed, highly aligned, multinucleated, and cross-striated myofibers surrounded by a basal lamina-like matrix consisting of laminin

---

Significance

Engineering of highly functional skeletal muscle tissues can provide accurate models of muscle physiology and disease and aid treatment of various muscle disorders. Previous tissue-engineering efforts have fallen short of recreating structural and contractile properties of native muscle in vitro. Here, we describe the creation of biomimetic skeletal muscle tissues with structural, functional, and myogenic properties characteristic of native muscle and contractile stress values that surpass those of neonatal rat muscle. When implanted and real-time imaged in live animals, engineered muscle grafts undergo robust vascularization and perfusion, exhibit continued myogenesis, and show further improvements in intracellular calcium handling and contractile function. This process is significantly enhanced by myogenic predifferentiation and formation of aligned muscle architecture in vitro.
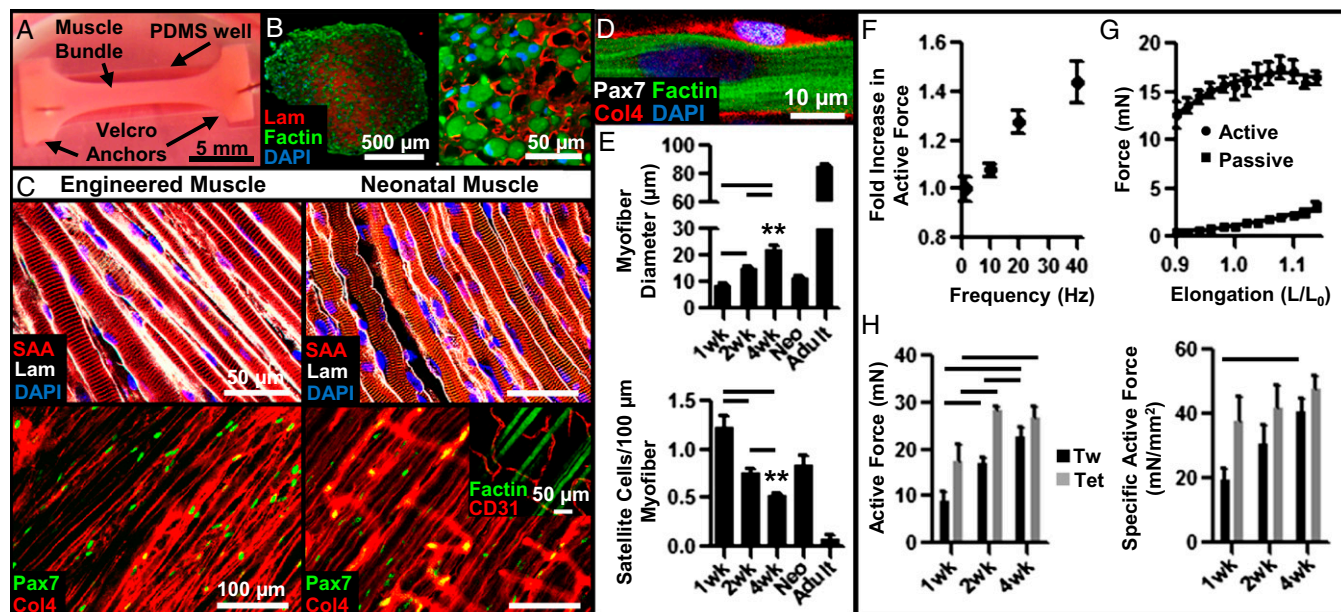
Fig. 1. Structural and functional characterization of in vitro-engineered skeletal muscle. (*A*) Live image of a 2-wk engineered muscle bundle (~1.5-mm diameter, 1.25 cm long) anchored at ends by tendon-mimetic Velcro tabs pinned inside a polydimethylsiloxane (PDMS) well. (*B*) Immunostained bundle cross-section shows F-actin$^+$ myofibers embedded within laminin (Lam)-rich matrix. (*C*) Structural organization of representative engineered and native neonatal rat soleus muscles. (*Inset*) Transverse Col4$^+$ structures present in native but not engineered muscle are CD31$^+$ blood vessels. Col4, collagen IV; SAA, sarcomeric α-actin. (*D*) Pax7$^+$ satellite cells in engineered muscle reside at myofiber sarcolemma. (*E*) Average myofiber diameter and SC number per 100-μm myofiber length at 1, 2, and 4 wk of culture compared with native neonatal (Neo) and adult soleus muscles. (*F*) Dependence of active force amplitude (normalized to that of single twitch) on stimulus frequency. (*G*) Dependence of active twitch and passive tension amplitudes on engineered muscle length (expressed relative to culture length). (*H*) Absolute and specific (force per area) twitch (Tw) and tetanus (Tet, 40 Hz) amplitudes in engineered bundles at 1, 2, and 4 wk of culture. Mean ± SEM; n = 4–10 samples per group (8–10 images per sample); **$P < 0.01$ between 4-wk bundle and native muscles; $P < 0.05$ between denoted groups.

and collagen IV (Fig. 1*C*). Within the basal lamina, Pax7$^+$ SCs were found residing within a native-like niche, closely abutting myofiber sarcolemma (Fig. 1 *C* and *D*, *SI Appendix*, Fig. S2 *B* and *C*). Overall, the 3D organization of the engineered muscle bundle highly resembled that of a native muscle fascicle, while lacking higher-order structures including multifascicle organization, tendons, and neurovascular bed.

Myogenesis in Engineered Muscle. We further quantified the temporal changes in cell proliferation and expression of key myogenic transcription factors [Pax7, MyoD, and myogenin (MyoG)] during in vitro culture (*SI Appendix*, Fig. S3). At early stages of engineered muscle formation (day 2), a large majority of Pax7$^+$ cells (~75%) were activated and proliferating as evidenced by their expression of Ki67 (*SI Appendix*, Fig. S3 *A* and *B*). Simultaneously, the vast majority of early fusing cells or newly formed, multinuclear myotubes expressed MyoD, either with or without MyoG (*SI Appendix*, Fig. S3 *C* and *D*). By culture day 14, the cells expressing MyoD alone virtually disappeared and all myonuclei in the engineered muscle expressed MyoG, either alone (~80%) or together with MyoD (*SI Appendix*, Fig. S4*D*). The ~20% MyoG$^+$/MyoD$^+$ myonuclei located at the periphery or within existing myofibers indicated cells that were either primed for fusion or recently fused. By culture day 14, Pax7$^+$ cells (*SI Appendix*, Fig. S4*A*) remained in relatively high numbers (~20% of all cells) and, as expected, did not coexpress MyoG (*SI Appendix*, Fig. S2*C*). Virtually all of the Pax7$^+$ cells were also MyoD$^-$ and quiescent, with only a small fraction (~1.5%) expressing Ki67, suggesting that the engineered muscle attained a differentiated, homeostatic state.

The presence of MyoD$^+$ cells in the homeostatic engineered muscle (*SI Appendix*, Fig. S3*D*) suggested the existence of continuous cell growth and hypertrophy that, in native postnatal muscle, are supported by creation of new myonuclei via secondary fusion of SCs with myofibers (19). We therefore quantified the temporal changes in myofiber size and SC density

at 1, 2, and 4 wk of culture and found significant increase in myofiber diameter (1 wk, 8.73 ± 0.33 μm; 2 wk, 14.9 ± 0.87 μm; 4 wk, 22.2 ± 1.33 μm) accompanied by decreases in SC number per 100 μm of myofiber length (1 wk, 1.22 ± 0.12; 2 wk, 0.75 ± 0.05; 4 wk, 0.52 ± 0.02) (Fig. 1*E* and *SI Appendix*, Fig. S4), indicative of a functioning SC pool and continuous myogenesis. After 4 wk of culture, these parameters achieved values intermediate between those of neonatal and adult rat muscle tissues (Fig. 1*E*).

Function of Engineered Muscle. In response to electrical stimulation, engineered muscle bundles generated strong twitch contractions that, with increase in stimulus frequency, fused into a more forceful tetanic contraction (Fig. 1*F*, *SI Appendix*, Fig. S5*A*, and Movie S1). As characteristic of native muscle (20), lengthening of engineered muscle yielded a biphasic increase in the amplitude of active (contractile) force and a monotonic increase in passive tension (Fig. 1*G* and *SI Appendix*, Fig. S5*B*). The contractile force-generating capacity of engineered muscle increased with time of culture [1 wk, 8.83 ± 2.3 and 17.27 ± 3.6 mN; 2 wk, 17.08 ± 1.1 and 28.39 ± 0.92 mN; 4 wk, 22.79 ± 2.1 and 26.75 ± 2.3 mN (twitch and tetanus)] (Fig. 1*H*), attaining values more than an order of magnitude higher than those previously reported for other engineered muscle tissues (8, 11, 21–26). Specific tetanic force per unit muscle cross-sectional area of 47.9 ± 4.1 mN/mm^2 in 4-wk engineered bundles surpassed values reported for native neonatal rat soleus muscle (44 mN/mm^2) (20). Moreover, passive tension during 4-wk culture did not change significantly (*SI Appendix*, Fig. S5*C*), yielding high active-to-passive force ratios of ~10–15 (*SI Appendix*, Fig. S5*D*), characteristic of neonatal skeletal muscle (20, 27) and, to our knowledge, unmet in previous tissue-engineering studies.

Response of Engineered Muscle to in Vitro Injury. To further investigate the SC function within the engineered muscle, we used a cardiotoxin (CTX) injury assay to assess whether the SCs can support muscle self-repair in vitro. Homeostatic, 2-wk-old engineered muscle was exposed to 0.2 μM CTX for 6 h and allowed

to recover for 10 d. Consistent with in vivo reports (28), the CTX exposure resulted in immediate fragmentation of myofibers, cell death, and disruption of contractile elements, leading to a four-fold decrease in contractile-force generation (Fig. 2 and *SI Appendix*, Fig. S6). In response to injury, SCs in the engineered muscle underwent robust activation and proliferation such that, by 5 d postinjury, initially decreased Pax7^{+} and MyoD[+] cell numbers significantly increased beyond those present in the preinjury muscle, accompanied by a significant rise in the percentage of proliferating SCs (Ki67^{+}/Pax7^{+}) (Fig. 2B and *SI Appendix*, Fig. S6 A and B). By 10 d postinjury, numbers of Pax7^{+}, Ki67^{+}/Pax7^{+}, and MyoD^{+} cells decreased whereas the number of MyoG[+] myonuclei, the myofiber density, and the percentage of cross-striated myofibers increased to near preinjury levels (Fig. 2B). The progressive regrowth, differentiation, and sarcomerogenesis of engineered muscle fibers resulted in steady recovery of both twitch and tetanic force generation that, by 10 d post-CTX injury, reached near preinjury levels (Fig. 2B).

Vascularization of Implanted Engineered Muscle. To assess the ability of the engineered muscle to survive and vascularize in vivo, we implanted 2-wk predifferentiated (PreD) bundles into a dorsal skinfold window chamber in nude mice (29). For this purpose, we generated smaller three-bundle constructs anchored within a single 9 × 9-mm square Cerex frame that fit within the window chamber (Fig. 3A). As a comparison group, we implanted un-differentiated (UnD) muscle bundles cultured for only 2 d without switching to differentiation media that contained sporadically fusing myotubes and high numbers of Pax7^{+} and Ki67^{+} cells (*SI Appendix*, Fig. S7). Placing the engineered muscle between the thin panniculus carnosus muscle layer of the dorsal skin and a cover glass window allowed us to nondestructively, in live animals, track angiogenesis and perfusion of the muscle implant in real time. With time post implantation (PI), initially avascular muscle bundles underwent rapid invasion by host blood vessels (Fig. 3B, yellow pseudocolored region) at a rate that was greater in PreD than in UnD muscle implants, which showed apparent saturation of vessel ingrowth by 14 d PI (Fig. 3C). Importantly, all ingrown capillary networks appeared functional and perfused by

host blood flow (evident from red blood cell motion) as early as 7 d PI (Movie S2). Interestingly, although asynchronous spontaneous twitches recorded at 2 wk PI had no apparent effect on the blood flow through ingrown capillaries, occasionally observed spontaneous tetanic contractions appeared to transiently restrict blood perfusion (Movie S3).

Immunostaining analysis (Fig. 3D) further revealed randomly oriented vessel networks at the periphery of implanted muscle whereas, within the implant interior, the ingrown capillaries coaligned with surrounding myofibers to a degree (4.97 ± 1.8°) characteristic of native neonatal muscle (*SI Appendix*, Fig. S8). In addition, in transverse cross-sections, endothelialized vessel lumens were found throughout the full thickness of the implants (Fig. 3E). In agreement with intravital imaging analysis, cross-sectional lumen density in both PreD and UnD implant regions increased between 1 wk (PreD, 170 ± 11 per mm^2; UnD, 75 ± 10 per mm^2) and 2 wk (PreD, 265 ± 30 per mm^2; UnD, 175 ± 18 per mm^2) PI and was significantly higher in PreD implants (Fig. 3F). From cross-sectional immunostainings, the average rate of vascular ingrowth in PreD muscle bundles was 18.9 ± 2.1 vessels·mm^{-2}·d^{-1}. Further, mean lumen diameter increased with time PI, and, after 2 wk, amounted to 7.1 ± 0.2 μm, similar to values measured in native hindlimb muscle (*SI Appendix*, Fig. S9).

Myogenesis in Implanted Engineered Muscle. After 2 wk in vivo, implanted PreD muscle bundles (identified by GFP[+] staining for GCaMP3) remained separated from the underlying host muscle and appeared to maintain preimplantation volume and a structure consisting of aligned cross-striated myofibers surrounded by basal lamina proteins (Fig. 3 G–I). Importantly, the implanted myofibers remained abutted by Pax7^{+} satellite cells at 2 wk PI, suggesting continued myogenic capacity of engineered muscle in vivo (Fig. 3J). Compared with preimplantation values [i.e., 2-wk in vitro culture (IVC)], PreD bundles at 1 wk PI had fewer cross-striated myofibers (−40.0 ± 7%); however, by 2 wk PI, virtually all myofibers exhibited cross-striations (*SI Appendix*, Fig. S10) whereas the PreD myofiber diameter became significantly increased (+40.7 ± 5% relative to IVC). Control UnD muscle bundles that before implantation showed only sporadic myofiber formation (*SI Appendix*, Figs. S7 and S10A) underwent significant myogenesis over 2 wk PI; however, their myofiber organization, alignment, diameter, and percent of cross-striated myofibers remained inferior to those of the PreD implants (*SI Appendix*, Figs. S10B and S11).

Function of Implanted Engineered Muscle. To nondestructively monitor viability and functionality of the engineered muscle in vivo, we lentivirally transduced intracellular Ca^{2+} sensor GCaMP3 (17) in isolated myogenic cells, which allowed us to record spontaneous and electrically induced Ca^{2+} transients in muscle implants by measuring GCaMP3 fluorescence (ΔF/F) (*SI Appendix*, Fig. S12 A–E). Intravital GCaMP3 fluorescence movies during spontaneous twitching of implanted muscle (Movie S4 and Fig. 4A) revealed that, after an initial lag period of ∼7 d, the PreD muscle implants exhibited a steady increase in Ca^{2+} transient amplitude (Fig. 4B). The UnD implants, with limited functionality at 2 d PI, also exhibited a steady increase in spontaneous activity and amplitude of Ca^{2+} transients (Fig. 4B). Measurements of electrically induced Ca^{2+} responses in explanted muscle (Movie S5) showed that, at 2 wk PI, both PreD and UnD muscle bundles displayed significantly greater Ca^{2+} transient amplitudes compared with their IVC and 1-wk PI counterparts (Fig. 4C). Kinetics of GCaMP3 Ca^{2+} transients were not significantly changed between 1 and 2 wk PI and were comparable between the two implant groups (*SI Appendix*, Fig. S13A).

Because the implanted engineered muscle underwent robust vascular integration with the host dorsal skin, it could not be separated from the skin without being damaged. Therefore, to eliminate host contribution to the measured contractile force, we implanted engineered muscle bundles in the direction perpendicular to that of the host panniculus carnosus muscle layer
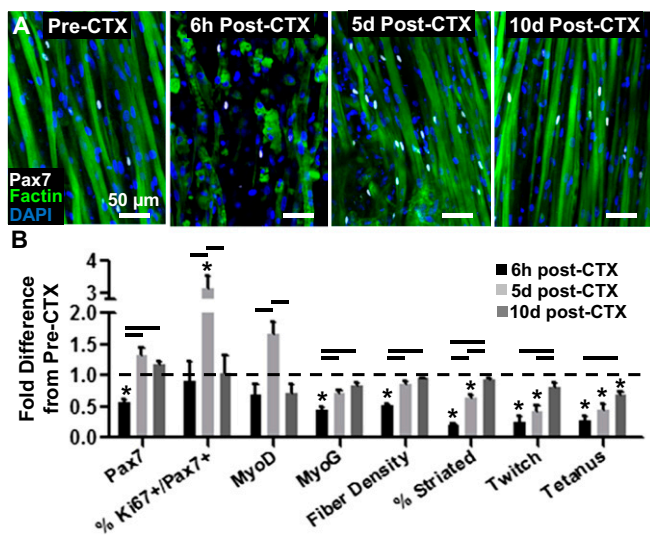
Fig. 2. Regenerative response of engineered muscle to in vitro cardiotoxin (CTX) injury. (A) Representative images of engineered muscle structure, and Pax7^{+} cells with time post-CTX injury (induced at 14 d of culture). (B) Pax7^{+}, Ki67^{+}/Pax7^{+} (% of Pax7^{+}), MyoD[+], and myogenin (MyoG)[+] cell density, myofiber density, percent cross-striated myofibers, and twitch and tetanus force amplitudes shown relative to preinjury levels at 6 h, 5 d, and 10 d post-CTX addition. Mean ± SEM; n = 3–5 samples per group (6–10 images per sample); *P < 0.05 compared with 2-wk healthy controls; P < 0.05 between denoted groups.

Fig. 3. Vascular integration of implanted engineered muscle. (*A*) Implanted muscle patch within the dorsal skin-fold window chamber. (*B*) Images of total hemoglobin at day 2, 9, and 14 in window chamber (yellow, implant region). (*C*) F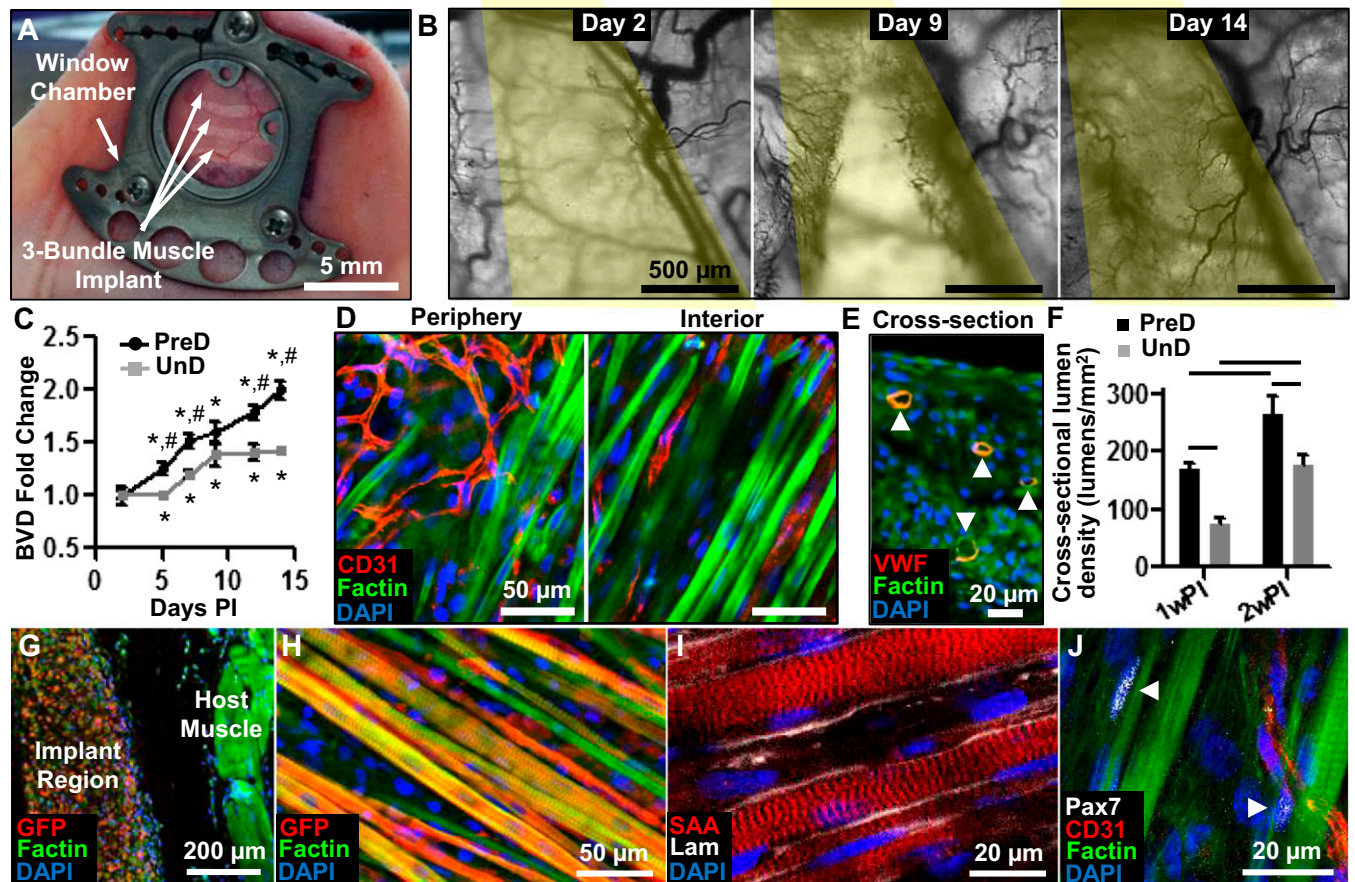old change in blood-vessel density (BVD) in the implant region of predifferentiated (PreD) and undifferentiated (UnD) bundles with time PI. (*D*) Vessel organization at the periphery and interior of muscle implant. CD31 labels endothelial cells. (*E*) Cross-section of the muscle implant showing lumens of ingrown blood vessels (arrowheads). VWF, von Willebrand factor. (*F*) Increase of cross-sectional BVD from 1 wk PI to 2 wk PI. (*G*) Cross-section of implant region (GFP-positive myofibers) and underlying host muscle. (*H* and *I*) Longitudinal section of implanted bundle showing aligned and cross-striated myofibers (*H*) embedded in laminin matrix (*I*). (*J*) Pax7$^+$ satellite cells (arrowheads) are found at the periphery of implanted myofibers. Mean ± SEM; n = 8–12 per group; *P < 0.05 from value at day 2, #P < 0.05 between PreD and UnD groups at same time point, P < 0.05 between groups denoted by horizontal lines.

(*SI Appendix*, Fig. S13 *F–H*). Functional measurements in 1- and 2-wk explants revealed robust contractile-force responses in both UnD and PreD groups (Fig. 4*D*). Specifically, implanted engineered UnD muscle steadily increased its force-generating capacity in vivo, and, after 2 wk PI, reached values similar to those measured in the PreD group before implantation (Fig. 4*E*). The implanted PreD muscle showed no enhancement in contractile-force generation during the first wk PI; however, its force-generating capacity significantly increased by 2 wk PI, reaching tetanus amplitudes 3.2-fold higher than the pre-implantation values. This significant increase in the absolute contractile-force amplitude was associated with an ~3.8-fold increase in specific force, which, at 2 wk PI, averaged 65.7 ± 8.9 mN/mm^2. Similar to Ca^{2+} transients, the kinetics of force generation in muscle implants did not significantly change between 1 and 2 wk PI and was comparable between the two implant groups (*SI Appendix*, Fig. S13). Overall, measurements of both Ca^{2+} transient and active force generation suggested that, in addition to robust vascularization, implanted engineered muscle underwent significant enhancement of contractile function in vivo, beyond what was achievable in vitro.

Discussion

In this study, we sought to reproduce important aspects of skeletal muscle organogenesis in vitro and create biomimetic tissue constructs with structural, functional, and myogenic properties characteristic of native muscle. Optimizing the cellular and extracellular cues essential for muscle growth and development, we created a 3D culture environment primed for myogenic maturation. Within this engineered muscle environment, initially proliferating Pax7$^+$ and MyoD$^+$ cells underwent rapid fusion and formation of aligned MyoG$^+$ myofibers that attained a highly differentiated phenotype and became surrounded by quiescent Pax7$^+$ SCs residing in native-like niches. Differentiation of SCs during 4-wk culture contributed to myofiber hypertrophy, a process characteristic of postnatal muscle growth (19). Along with the structural maturation, the contractile capacity of engineered muscle increased beyond specific force values measured in neonatal rat muscle, reaching contractile-force amplitude (~30 mN) 10–100 times higher than previously achieved (8, 11, 21–26).

To assess the self-regenerative capacity of engineered muscle, we perturbed its homeostatic state by a short exposure to cardiotoxin, causing significant cell death, myofiber fragmentation, and decline in functional output. Similar to injury response in vivo (30, 31), quiescent SCs in engineered muscle underwent rapid activation and myogenesis to yield efficient structural repair and restoration of contractile function, followed by recovery of myogenic indices to preinjury values. Collectively, by its ability to support native-like SC function, the 3D engineered muscle tissue described herein may facilitate systematic in vitro studies of SC fate during simulated growth, exercise, injury, or disease (30, 32).
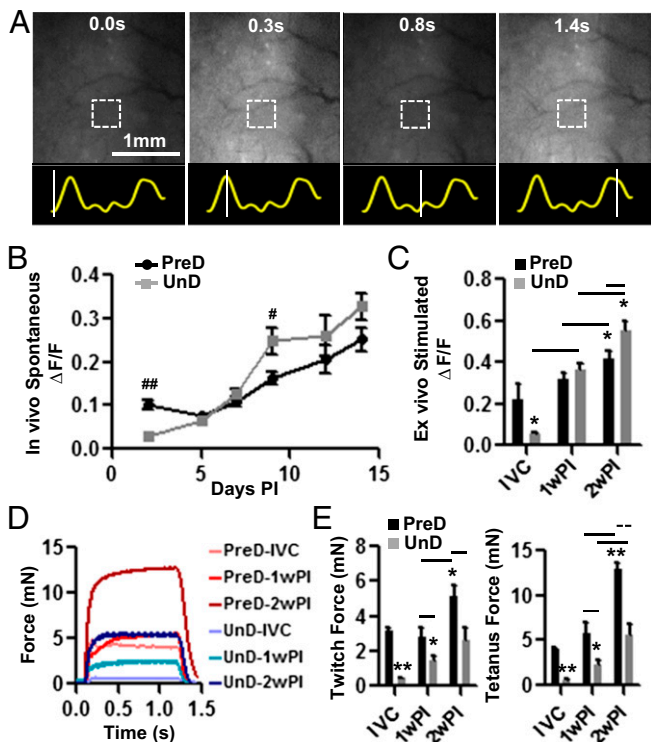
Fig. 4. Calcium transients and force generation of implanted engineered muscle. (*A*) Representative intravital snapshots of a GCaMP3 movie recorded during spontaneous activity of an implanted muscle bundle. Traces below panels show time course of GCaMP3 signal from a small bundle region (square) with lines denoting the snapshot times. Average amplitudes of in vivo spontaneous (*B*) and ex vivo electrically induced (*C*) GCaMP3 transients in implanted PreD and UnD engineered muscle with time PI. IVC, 2 wk of in vitro culture, before implantation. Representative tetanus force traces (*D*) and quantified (*E*) twitch and tetanus force amplitudes for PreD and UnD muscle cultured in vitro (IVC) or explanted at 1 wk PI and 2 wk PI. Mean ± SEM; n = 6–12 bundles per group; #P < 0.05 and ##P < 0.001 between PreD and UnD group at same time point; *P < 0.05 and **P < 0.001 compared with PreD IVC group; P < 0.05 and P < 0.001 between groups identified by horizontal solid and dashed lines, respectively.

To explore the fate of engineered muscle in vivo, we further combined GCaMP3 transduction with dorsal window chamber studies in live mice and noninvasively monitored the ability of implanted engineered muscle to spontaneously contract, generate Ca^{2+} transients, and undergo blood perfusion over a 2-wk period postimplantation. Regarding the rapid development of new fluorescent biosensors of cellular function and signaling (e.g., intracellular ion concentrations, membrane potential, cAMP, pH, etc.) (33, 34), we expect that similar experimental frameworks could allow real-time in vivo studies of various cellular processes of importance for the fields of stem-cell and cancer biology, tissue engineering, immunology, and others. In particular, the described concept of simultaneous monitoring of cell viability, intracellular Ca^{2+} concentration, and vascularization within a window-chamber environment could be directly applied to in vivo studies of Ca^{2+} oscillation-dependent differentiation and function of the heart, neuronal, pancreatic, intestinal, and other cellular and tissue implants.

In our in vivo studies, implanted engineered muscle, showing no evidence of vascular cells at the time of implantation, became progressively infiltrated with host blood vessels and, as evidenced by video-imaging (Movie S2), actively perfused with readily discernible blood cells by 7 d PI. By day 14, the vessel density within the PreD muscle implant (265 ± 30 vessels per mm^2) was comparable with that previously reported for implanted tissue-engineered muscle with preformed vascular structures (11), demonstrating that purely

angiogenic vessel ingrowth was sufficient to support the in vivo survival and function of small size avascular engineered muscles used in our study. On the other hand, successful survival of large engineered muscle implants will likely require the development of novel methods for in vitro fabrication of highly aligned, functional, and prevascularized skeletal muscle tissues. In a related finding, our preliminary data demonstrate that simple coencapsulation of myogenic and endothelial cells may significantly impair the contractile function of engineered muscle (*SI Appendix*, Fig. S14), suggesting that angiogenic vessel ingrowth, rather than simple vasculogenesis, may be a desired mode of engineered muscle vascularization, compatible with the formation of biomimetic muscle architecture and function in vitro.

Previously, various cell-based approaches have been explored for treatment of muscle injury or disease (30). Specifically, implanted freshly isolated SCs were found to fuse to existing myofibers, rescue contractile function, and, by homing to the host niche, enhance muscle capacity for endogenous self-repair (14–16). Still, without development of more efficient methods for their expansion in vitro (35, 36), implanted SCs may not be able to undergo timely myogenesis to successfully repair large muscle loss (37). Implanting readily expandable myoblasts or predifferentiated myofibers may accelerate in vivo myogenesis whereas codelivery of growth factors may improve cell survival and engraftment (12); however, without SCs, such strategies are likely to provide a limited support for future regenerative events (14, 15, 35). In the current study, we compared the post-implantation fate of PreD muscle constructs consisting of differentiated myofibers and functional SCs with UnD constructs consisting of undifferentiated, proliferative myogenic cells. We found that PreD implants not only exhibited superior structural and functional maturation (evidenced by larger myofiber diameter, percent cross-striations, and contractile force) (Fig. 4 and *SI Appendix*, Figs. S10 and S11) but also attracted significantly more neovessel ingrowth than UnD implants (Fig. 3 *C* and *F*), possibly due to the increased metabolic demand of more functional myofibers (38). Although these studies used a small implant size inadequate for therapeutic muscle replacement, they suggest the potential benefits of implanting a functional engineered muscle in which mature myofibers provide a niche-like environment for satellite cells compared with the sole use of undifferentiated myogenic cells.

Despite a steady increase in vascularization (Fig. 3*C*), the amplitude of spontaneous Ca^{2+} transients in engineered muscle implants started to steadily increase (and correlate with vascular ingrowth) (39) only after an initial lag period of 1 wk (Fig. 4*B*). Furthermore, the percentage of cross-striated fibers in PreD implants at 1 wk PI was decreased compared with the pre-implantation values (*SI Appendix*, Fig. S10*B*). This adaptation period may have resulted from potential tissue damage caused by initial hypoxia upon implantation into the dorsal window chamber and/or disruption of cell–matrix interactions caused by increased fibrinolysis (in the absence of the antifibrinolyitc supplement amino-caproic acid present in vitro) (26). Nevertheless, by 2 wk PI, continuous vascularization, myogenesis, and differentiation of the PreD implants led to an ~threefold increase in force-generating capacity compared with preimplantation values (Fig. 4*E*), yielding specific contractile forces of ~70 mN/mm^2. This in vivo recovery of the engineered muscle function and structural organization followed a similar time course to that observed in vitro upon CTX-induced injury. Along with the maintenance of aligned, cross-striated myofiber architecture (Fig. 3*I*) and satellite cell pool (Fig. 3*J*), vascularized engineered muscle implants in our study, for the first time, to our knowledge, exhibited structure, contractile function, and myogenic capacity representative of postneonatal skeletal muscle.

In summary, we presented a platform for engineering and studying of highly biomimetic skeletal muscle tissues with functional satellite cells capable of supporting myogenic and self-regenerative events characteristic of native muscle. Although initially avascular, these engineered muscle tissues underwent robust

vascularization and perfusion and exhibited continued myogenesis and improved contractile function in vivo, all of which were significantly enhanced by myogenic predifferentiation of tissue constructs in culture. Together, these results lay a foundation for novel in vitro and in vivo studies of skeletal muscle function, regeneration, and vasculogenesis and provide a blueprint for future engineering of 3D functional human muscle microtissues for drug and toxicology studies (4, 40).

Materials and Methods

All methods are described in detail in *SI Appendix*.

Engineering of Muscle Bundles. Large single muscle bundles and smaller tribundle muscle implants were formed within polydimethylsiloxane (PDMS) molds as previously described (26, 41). Cell/hydrogel mixture (*SI Appendix*, Table S1) was injected into the PDMS molds, polymerized at 37 °C for 45 min, and cultured on a rocker at 37 °C for up to 4 wk.

In Vitro Cardiotoxin Injury Assay. Following 2 wk of in vitro culture, differentiated engineered muscle bundles were exposed to 0.2 μM cardiotoxin (CTX) (cardiotoxin from *Naja mossambica mossambica*; Sigma) for 6 h on a rocker at 37 °C. The injured bundles were then rinsed three times to remove the toxin and reincubated in fresh differentiation medium. Cardiotoxin-injured bundles were assessed for structural composition and contractile function immediately after CTX removal (6 h post-CTX group) and after culture in differentiation media for an additional 5 or 10 d (5 d post-CTX and 10 d post-CTX groups).

Implantation of Engineered Muscle. All animal experiments were approved by the Duke University Animal Care and Use Committee. A circular region (~12 mm) of the forward-facing dorsal skin of nude mice was dissected away, and a tribundle muscle construct was laid perpendicular to the muscle on the rearward-facing skin (*SI Appendix*, Fig. S14), providing a source of host microvessels (29).

Intravital Imaging of Blood Vessels and Intracellular Ca^{2+} Transients. Intravital recordings were performed at 5× magnification on days 2, 5, 7, 9, 12, and 14 postimplantation (PI). Capillary vessels were imaged by a video camera and analyzed from total hemoglobin images (29). Spontaneous Ca^{2+} transients reported by GCaMP3 (17) fluorescence were imaged by a fast CCD camera and analyzed as previously described (25).

In Vitro and ex Vivo Force Measurements. Engineered muscle constructs were loaded into a custom-made force-measurement setup containing an optical force transducer and a linear actuator (ThorLabs), as previously described (25, 26, 42). Samples were stimulated (10 ms, 3 V/mm pulses) at different frequencies (1–40 Hz), and isometric passive and active (contractile) forces were measured at different muscle lengths. Kinetics of contraction and specific force were calculated as previously described (26).

1. Kuang S, Chargé SB, Seale P, Huh M, Rudnicki MA (2006) Distinct roles for Pax7 and Pax3 in adult regenerative myogenesis. *J Cell Biol* 172(1):103–113.
2. Lepper C, Partridge TA, Fan CM (2011) An absolute requirement for Pax7-positive satellite cells in acute injury-induced skeletal muscle regeneration. *Development* 138(17):3639–3646.
3. Cosgrove BD, Sacco A, Gilbert PM, Blau HM (2009) A home away from home: Challenges and opportunities in engineering in vitro muscle satellite cell niches. *Differentiation* 78(2-3):185–194.
4. Vandenburgh H (2010) High-content drug screening with engineered musculoskeletal tissues. *Tissue Eng Part B Rev* 16(1):55–64.
5. Juhas M, Bursac N (2013) Engineering skeletal muscle repair. *Curr Opin Biotechnol* 24(5):880–886.
6. Rossi CA, Pozzobon M, De Coppi P (2010) Advances in musculoskeletal tissue engineering: Moving towards therapy. *Organogenesis* 6(3):167–172.
7. Shansky J, Del Tatto M, Chromiak J, Vandenburgh H (1997) A simplified method for tissue engineering skeletal muscle organoids in vitro. *In Vitro Cell Dev Biol Anim* 33(9):659–661.
8. Dennis RG, Kosnik PE, 2nd (2000) Excitability and isometric contractile properties of mammalian skeletal muscle constructs engineered in vitro. *In Vitro Cell Dev Biol Anim* 36(5):327–335.
9. Levenberg S, et al. (2005) Engineering vascularized skeletal muscle tissue. *Nat Biotechnol* 23(7):879–884.
10. Thorrez L, et al. (2006) Angiogenesis enhances factor IX delivery and persistence from retrievable human bioengineered muscle implants. *Mol Ther* 14(3):442–451.
11. Koffler J, et al. (2011) Improved vascular organization enhances functional integration of engineered skeletal muscle grafts. *Proc Natl Acad Sci USA* 108(36):14789–14794.
12. Borselli C, Cezar CA, Shvartsman D, Vandenburgh HH, Mooney DJ (2011) The role of multifunctional delivery scaffold in the ability of cultured myoblasts to promote muscle regeneration. *Biomaterials* 32(34):8905–8914.
13. Corona BT, Ward CL, Baker HB, Walters TJ, Christ GJ (2014) Implantation of in vitro tissue engineered muscle repair constructs and bladder acellular matrices partially restore in vivo skeletal muscle function in a rat model of volumetric muscle loss injury. *Tissue Eng Part A* 20(3-4):705–715.
14. Montarras D, et al. (2005) Direct isolation of satellite cells for skeletal muscle regeneration. *Science* 309(5743):2064–2067.
15. Rossi CA, et al. (2011) In vivo tissue engineering of functional skeletal muscle by freshly isolated satellite cells embedded in a photopolymerizable hydrogel. *FASEB J* 25(7):2296–2304.
16. Sacco A, Doyonnas R, Kraft P, Vitorovic S, Blau HM (2008) Self-renewal and expansion of single transplanted muscle stem cells. *Nature* 456(7221):502–506.
17. Tian L, et al. (2009) Imaging neural activity in worms, flies and mice with improved GCaMP calcium indicators. *Nat Methods* 6(12):875–881.
18. Shiba Y, et al. (2012) Human ES-cell-derived cardiomyocytes electrically couple and suppress arrhythmias in injured hearts. *Nature* 489(7415):322–325.
19. Davis TA, Fiorotto ML (2009) Regulation of muscle growth in neonates. *Curr Opin Clin Nutr Metab Care* 12(1):78–85.
20. Close R (1964) Dynamic properties of fast + slow skeletal muscles of rat during development. *J Physiol* 173(1):74–95.
21. Yan W, et al. (2007) Tissue engineering of skeletal muscle. *Tissue Eng* 13(11):2781–2790.
22. Williams ML, Kostrominova TY, Arruda EM, Larkin LM (2013) Effect of implantation on engineered skeletal muscle constructs. *J Tissue Eng Regen Med* 7(6):434–442.
23. Huang YC, Dennis RG, Larkin L, Baar K (2005) Rapid formation of functional muscle in vitro using fibrin gels. *J Appl Physiol (1985)* 98(2):706–713.
24. Carosio S, et al. (2013) Generation of eX vivo-vascularized Muscle Engineered Tissue (X-MET). *Sci Rep* 3:1420.
25. Bian W, Bursac N (2012) Soluble miniagrin enhances contractile function of engineered skeletal muscle. *FASEB J* 26(2):955–965.
26. Hinds S, Bian W, Dennis RG, Bursac N (2011) The role of extracellular matrix composition in structure and function of bioengineered skeletal muscle. *Biomaterials* 32(14):3575–3583.
27. Mutungi G, Trinick J, Ranatunga KW (2003) Resting tension characteristics in differentiating intact rat fast- and slow-twitch muscle fibers. *J Appl Physiol (1985)* 95(6):2241–2247.
28. Couteaux R, Mira JC, d'Albis A (1988) Regeneration of muscles after cardiotoxin injury. I. Cytological aspects. *Biol Cell* 62(2):171–182.
29. Palmer GM, et al. (2011) In vivo optical molecular imaging and analysis in mice using dorsal window chamber models applied to hypoxia, vasculature and fluorescent reporters. *Nat Protoc* 6(9):1355–1366.
30. Yin H, Price F, Rudnicki MA (2013) Satellite cells and the muscle stem cell niche. *Physiol Rev* 93(1):23–67.
31. Dhawan J, Rando TA (2005) Stem cells in postnatal myogenesis: Molecular mechanisms of satellite cell quiescence, activation and replenishment. *Trends Cell Biol* 15(12):666–673.
32. Sacco A, et al. (2010) Short telomeres and stem cell exhaustion model Duchenne muscular dystrophy in mdx/mTR mice. *Cell* 143(7):1059–1071.
33. Tantama M, Hung YP, Yellen G (2012) Optogenetic reporters: Fluorescent protein-based genetically encoded indicators of signaling and metabolism in the brain. *Prog Brain Res* 196:235–263.
34. Okumoto S, Jones A, Frommer WB (2012) Quantitative imaging with fluorescent biosensors. *Annu Rev Plant Biol* 63:663–706.
35. Gilbert PM, et al. (2010) Substrate elasticity regulates skeletal muscle stem cell self-renewal in culture. *Science* 329(5995):1078–1081.
36. Urbani L, Piccoli M, Franzin C, Pozzobon M, De Coppi P (2012) Hypoxia increases mouse satellite cell clone proliferation maintaining both in vitro and in vivo heterogeneity and myogenic potential. *PLoS ONE* 7(11):e49860.
37. Turner NJ, Badylak SF (2012) Regeneration of skeletal muscle. *Cell Tissue Res* 347(3):759–774.
38. Fraisl P, Mazzone M, Schmidt T, Carmeliet P (2009) Regulation of angiogenesis by oxygen and metabolism. *Dev Cell* 16(2):167–179.
39. Lee SL, Pevec WC, Carlsen RC (2001) Functional outcome of new blood vessel growth into ischemic skeletal muscle. *J Vasc Surg* 34(6):1096–1102.
40. Truskey GA, et al. (2013) Design considerations for an integrated microphysiological muscle tissue for drug and tissue toxicity testing. *Stem Cell Res Ther* 4(Suppl 1, Suppl 1):S10.
41. Bian W, Liau B, Badie N, Bursac N (2009) Mesoscopic hydrogel molding to control the 3D geometry of bioartificial muscle tissues. *Nat Protoc* 4(10):1522–1534.
42. Liau B, Christoforou N, Leong KW, Bursac N (2011) Pluripotent stem cell-derived cardiac tissue patch with advanced structure and function. *Biomaterials* 32(35):9180–9187.

APPLIED BIOLOGICAL SCIENCES